Asian Journal of Chemistry; Vol. 38, No. 4 (2026), 1027-1037
ASIAN JOURNAL OF CHEMISTRY
https://doi.org/10.14233/ajchem.2026.35395

A New Class of 1,2,4-Triazolo-Benzothiazole Hybrids as Promising Antibacterial Agents

SURESH S. HONNALLI[1], GIRISH A. HAMPANNAVAR[1,*] and IRANNA S. GATIBYALI[2]

[1]Department of Pharmaceutical Chemistry, KLE College of Pharmacy, Vidyanagar, Hubballi-580031, India
[2]Department of Pharmaceutical Chemistry, KLE College of Pharmacy, Gadag-582101, India

*Corresponding author: E-mail: girihamp@gmail.com

Received: 4 December 2025 *Accepted*: 2 March 2026 *Published online*: 8 April 2026 AJC-22325

A novel series of 1,2,4-triazolo-benzothiazole derivatives (**6a-l**) were designed, synthesised and evaluated for antimicrobial activity. The synthesis proceeded through multistep construction of the triazolo-benzothiazole core from *m*-chloroaniline, followed by functionalisation with substituted aromatic and heterocyclic amines. Structures were confirmed by IR, NMR and mass spectrometry. Antibacterial screening against Gram-positive (*S. aureus*, *B. subtilis*) and Gram-negative (*E. coli*, *P. aeruginosa*) strains employed cup-plate and serial-dilution assays. Compounds **6a**, **6e** and especially **6h** displayed broad-spectrum potency, with **6h** active at low concentrations. Molecular docking showed strong binding where, **6e** scored -10.8 kcal/mol against *S. aureus* (PDB 5CPQ) and **6d** scored -10.5 kcal/mol against *E. coli* (PDB 5TZ1), surpassing ciprofloxacin (-8.0 and -8.5 kcal/mol, respectively). Interactions involved multiple hydrogen bonds and extensive hydrophobic contacts. ADMET profiling indicated compliance with Lipinski's rule of five, high gastrointestinal absorption, low toxicity risk and no blood-brain barrier penetration, supporting their potential as orally active antimicrobial agents.

Keywords: 1,2,4-Triazolo-benzothiazole, Heterocyclic synthesis, Antibacterial activity, Cup-plate method, Serial dilution method.

INTRODUCTION

1,2,4-Triazolo-benzothiazolyl derivatives represent a promising class of heterocyclic compounds that have gathered significant attention in medicinal chemistry due to their diverse pharmacological properties. The fusion of 1,2,4-triazole and benzothiazole moieties has been shown to exhibit a wide range of biological activities, including antimicrobial [1], antifungal [2], anti-inflammatory [3], anti-Alzheimer [4] and anticancer [5] properties. The unique structural features of these compounds, combined with their potential therapeutic benefits, make them an attractive target for further research and development.

1,2,4-Triazole scaffold, characterised by a five-membered heterocyclic ring containing three nitrogen atoms, exhibits notable chemical properties that contribute to its biological significance [6]. The inherent tautomerism of 1,2,4-triazoles allows dynamic structural transformations, influencing their reactivity and interactions with biomolecules [7]. Furthermore, these compounds can undergo nucleophilic substitution reactions, enabling the introduction of diverse functional groups and modulation of their pharmacological profiles. Also, 1,2,4-triazoles can form stable complexes with transition metals, which can enhance their biological activity by facilitating specific interactions with enzymes or receptors [8].

Benzothiazoles possess extended π-delocalised systems, enabling them to interact with DNA molecules through π-π stacking interactions [9]. This property contributes to their complex biological profiles, rendering them a valuable scaffold for drug design. Benzothiazole derivatives have been found to exhibit a range of pharmacological activities, including antitumor, neurotransmission blocking, antimicrobial and antifungal properties [10]. Moreover, they have been utilised as β-amyloid imaging agents, highlighting their versatility in the medicinal applications.

Considering the therapeutic potential of these heterocycles, the present work aims to hybridize 1,2,4-triazole and benzothiazole antimicrobial scaffolds, with the anticipation of developing more effective antimicrobial compounds. Despite extensive reports on the individual pharmacological activities of triazole and benzothiazole derivatives, limited efforts have been made to rationally hybridize these scaffolds into single molecular frameworks with optimised antimicrobial efficacy. Existing studies often examine these scaffolds separately, leaving a gap in understanding whether their combined

structural features can synergistically improve antibacterial activity. Addressing this gap, our work seeks to design and synthesise novel benzothiazolyl-triazole hybrids and evaluate their antimicrobial potential. The synthesised compounds were characterised by IR and NMR spectroscopic tools and the antibacterial activity evaluation was performed on Gram-positive and Gram-negative strains.

EXPERIMENTAL

All the chemicals were purchased from Sigma Aldrich, Rankem Chemicals, SD Fine-Chem Ltd and Spectrochem and used without further purification. Melting points of the synthesised compounds were determined in open capillaries on Equiptronics Digital melting point apparatus and are uncorrected. Reactions progress was monitored by thin-layer chromatography (TLC) on Silica gel 60 F_{254} aluminum sheets (Sigma-Aldrich). The mobile phase was *n*-hexane and ethyl acetate, 9:1 (v:v) and detection was made using UV light and iodine vapours. FT-IR spectra were recorded on Thermo Nicolet IR-200 spectrophotometer using as KBr pellets. ^{1}H NMR were recorded in $CDCl_3$ or DMSO-d_6 solvent on a Bruker Avance II NMR 400 MHz instrument (400.1324 MHz for ^{1}H and 100.62 MHz for ^{13}C). Mueller Hinton Agar media and Mueller-Hinton Broth were procured from Hi-Media, and DMSO was purchased from Sigma-Aldrich.

Synthesis of 7-chlorobenzo[*d*]thiazol-2-amine (1): A solution of *m*-chloroaniline (30 mmol) in 95% acetic acid (20 mL) was added to a solution of KSCN (120 mmol) in 95% acetic acid (20 mL). The reaction mixture was cooled to 0 ºC and a solution of bromine (1.6 mL) in acetic acid (10 mL) was added over 1.5 h. During the addition, the temperature was maintained below to 5 ºC. After complete addition of bromine, the stirring was continued additionally for 3 h at 10-15 ºC and then the reaction mixture was poured into hot water (300 mL). Separated hydrochloride salt was filtered and washed with acetic acid and dried. The obtained solid was later dissolved in hot water and neutralised with 26% ammonium hydroxide solution. The obtained solid was filtered and washed with water and recrystallised in ethanol. The progress of the reaction was monitored by TLC using *n*-hexane and EtOAc (9:1) using iodine vapours as visualizing agent. Yield: 90%, m.p.: 178-180 ºC. R_f: 0.64. FT-IR (KBr, ν_{max}, cm^{-1}): 3390 (NH-*str*.), 1424 (Ar-C=C), 1652 (C=N), 779 (C-Cl); ^{1}H NMR (DMSO-d_6, δ ppm): 7.59 (m, 1H, Ar-H), 7.48 (s, 2H, NH_2), 7.28-7.30 (m, 1H, Ar-H), 7.15-7.17 (m, 1H, Ar-H).

Synthesis of ethyl-(7-chlorobenzo[*d*]thiazol-2-yl)carbamate (2): Compound **1** (0.001 mol) was dissolved in minimum amount of pyridine (~ 2 mL) and cooled to 0 ºC under anhydrous conditions. Ethyl chloroformate (0.001 mol) was added dropwise to the previous solution by maintaining the temperature at 0-2 ºC with constant stirring under anhydrous conditions for about 1 h. Further, after stirring for about 0.5 h at room temperature, the reaction mixture was heated for 12 h on a water bath. The contents were then poured with stirring into ice water and the pyridine was removed by steam distillation. The obtained solid was filtered, dried and purified by recrystallisation from absolute ethanol to yield colourless crystalline compound. The progress of the reaction was monitored by TLC using *n*-hexane and EtOAc (9:1). Yield: 66%, m.p.: 230-232 ºC. R_f: 0.44. FT-IR (KBr, ν_{max}, cm^{-1}): 3174 (NH-*str*.), 1551 (Ar-C=C), 1732 (C=N), 758 (C-Cl); ^{1}H NMR (DMSO-d_6, δ ppm): 7.53 (m, 1H, Ar-H), 7.39 (s, 1H, NH), 7.28-7.30 (m, 1H, Ar-H), 7.15-7.17 (m, 1H, Ar-H), 4.21 (m, 2H, -CH_2), 1.37 (m, 3H, -CH_3).

Synthesis of *N*-(7-chlorobenzo[*d*]thiazol-2-yl)hydrazinecarboxamide (3): A suspension of compound **2** (0.001 mol) in ethanol (10 mL) was refluxed with hydrazine hydrate (2 mL, 99%) on a water bath for 9 h. The reaction mixture was cooled to room temperature to offer a white solid, which was filtered, dried and purified by recrystallisation from ethanol to get colourless crystalline compound. The progress of reaction was monitored using TLC (*n*-hexane:EtOAc, 9:1). Yield: 60%, m.p.: 150-152 ºC. R_f: 0.32. FT-IR (KBr, ν_{max}, cm^{-1}): 3455 (NH-*str*.), 1444 (Ar-C=C), 1632 (C=N), 765 (C-Cl); ^{1}H NMR (DMSO-d_6, δ ppm): 9.69 (s, 1H, NH), 4.62 (m, 2H, NH_2), 7.53 (m, 1H, Ar-H), 7.39 (s, 1H, NH), 7.28-7.30 (m, 1H, Ar-H), 7.15-7.17 (m, 1H, Ar-H).

Synthesis of 7-chloro-*N*-(4*H*-1,2,4-triazol-3-yl)benzo[*d*]thiazol-2-amine (4): A mixture of acetonitrile (3 mmol), hydrazide derivative (**3**) (1 mmol) and K_2CO_3 (0.5 mmol) in butanol (2 mL) was placed in a round bottom flask and the temperature was set to 150 ºC, in an oil bath and refluxed for 14 h. After completion, the mixture was evaporated to obtain solid which was recrystallised with methanol. The progress of reaction was ascertained by TLC (*n*-hexane:EtOAc, 9:1). Yield: 65%, m.p.: 135-137 ºC. R_f: 0.35. FT-IR (KBr, ν_{max}, cm^{-1}): 3453 (NH-*str*.), 1440 (Ar-C=C), 1534 (C=N), 758 (C-Cl); ^{1}H NMR (DMSO-d_6, δ ppm): 9.69 (s, 1H, NH), 6.78-7.96 (m, 5H, Ar-H).

Synthesis of 7-chloro-*N*-(5-(4-ethoxyphenyl)-4*H*-1,2,4-triazol-3-yl)benzo[*d*]thiazol-2-amine (5): A mixture of 13.9 g (0.05 mol) of compound **4** and 8.26 g (0.05 mol) of *p*-ethoxybenzoic acid in pyridine (100 mL) was heated at 170-210 ºC for 4 h in an oil bath under moisture free conditions. The fused material after cooling was treated with cold sodium bicarbonate solution (10%). The resulting solution was filtered, washed and recrystallised from methanol. The prog-ress of reaction was monitored using TLC (*n*-hexane:EtOAc; 9:1). Yield: 65%, m.p.: 160-162 ºC. R_f: 0.51. FT-IR (KBr, ν_{max}, cm^{-1}): 3453 (NH-*str*.), 1419 (Ar-C=C), 1603 (C=N), 777 (C-Cl); ^{1}H NMR (DMSO-d_6, δ ppm): 9.69 (s, 1H, NH), 6.78-7.96 (m, 7H, Ar-H), 4.02 (s, 1H, NH), 3.52-3.57 (m, 2H, -CH_2), 1.27-1.43 (m, 3H, CH_3).

General procedure for synthesis of N^2-(5-(4-ethoxyphenyl)-4*H*-1,2,4-triazol-3-yl)-N^7-phenylbenzo[*d*]thiazole-2,7-diamine derivatives (6a-l): An equimolar mixture of compound **5** (0.0025 mol) and various substituted aromatic amines (0.0025 mol) were refluxed for 2 h in DMF. The reaction mixture was allowed to cool and poured into the crushed ice with rigorous stirring (**Scheme-I**). The solid separated was filtered off, dried and recrystallised from benzene and absolute alcohol (1:1). The progress of reaction was monitored using TLC (*n*-hexane:EtOAc; 9:1).

N^2-(5-(4-Ethoxyphenyl)-4*H*-1,2,4-triazol-3-yl)-N^7-(2-nitrophenyl)benzo[*d*]thiazole-2,7-diamine (6a): Yield: 80%,

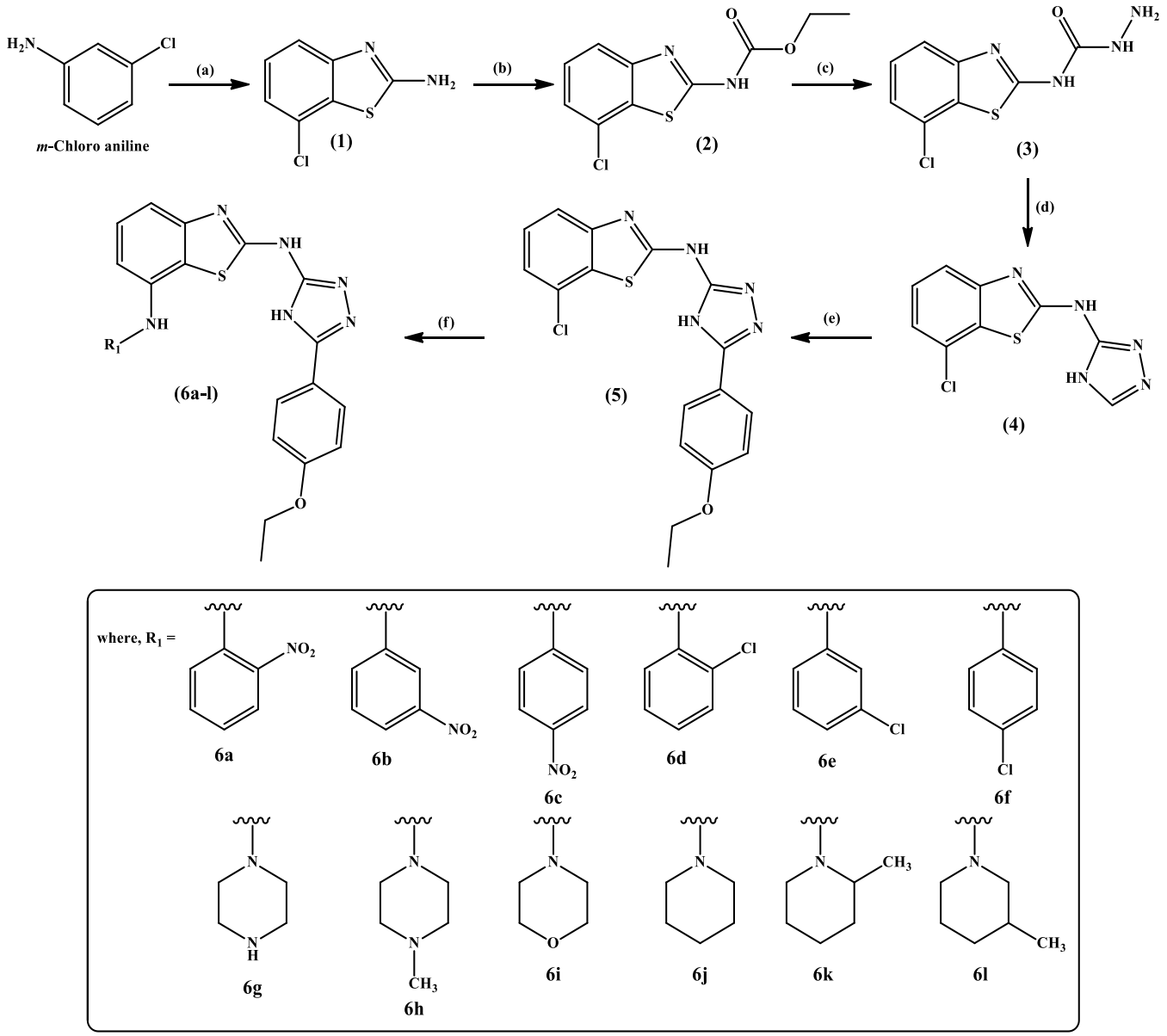

Scheme-I: Synthesis of 1,2,4-Triazolo-Benzothiazole Hybrids (**6a-l**): Reactions & conditions (a) KSCN, CH_3COOH, Br_2, NH_3; (b) ethyl chloroformate, pyridine; (c) $NH_2{\cdot}NH_2{\cdot}H_2O$, reflux (9 h); (d) CAN, K_2CO_3, butanol, 150 ºC, reflux (14 h); (e) *p*-ethoxybenzoic acid, pyridine, 170-210 ºC (4 h); (f) substituted primary amines, DMF, reflux (2 h)

m.p.: 236-238 ºC. R_f: 0.79. FT-IR (KBr, ν_{max}, cm^{-1}): 3416 (NH-*str*.), 1623 (C=N), 1538 (Ar-NO_2), 1428 (Ar-C=C); ^{1}H NMR (DMSO-d_6, δ ppm): 8.76 (s, 1H, Ar-NH), 6.58-7.86 (m, 12H, Ar-H), 4.12 (s, 1H, NH), 2.90-3.07 (m, 2H, -CH_2), 1.07-1.10 (m, 3H, CH_3).

***N*^{2}-(5-(4-ethoxyphenyl)-4*H*-1,2,4-triazol-3-yl)-*N*^{7}-(3-nitrophenyl)benzo[*d*]thiazole-2,7-diamine (6b):** Yield: 82%, m.p.: 232-234 ºC. R_f: 0.85. FT-IR (KBr, ν_{max}, cm^{-1}): 3463 (NH-*str*.), 1623 (C=N), 1538 (Ar-NO_2), 1489 (Ar-C=C); ^{1}H NMR (DMSO-d_6, δ ppm): 8.73 (s, 1H, Ar-NH), 6.53-7.81 (m, 12H, Ar-H), 4.08 (s, 1H, NH), 2.92-3.04 (m, 2H, -CH_2), 1.03-1.09 (m, 3H, CH_3).

***N*^{2}-(5-(4-ethoxyphenyl)-4*H*-1,2,4-triazol-3-yl)-*N*^{7}-(4-nitrophenyl)benzo[*d*]thiazole-2,7-diamine (6c):** Yield: 83%, m.p.: 224-226 ºC. R_f: 0.86. FT-IR (KBr, ν_{max}, cm^{-1}): 3410 (NH-*str*.), 1591 (C=N), 1531 (Ar-NO_2), 1424 (Ar-C=C); ^{1}H NMR (DMSO-d_6, δ ppm): 8.69 (s, 1H, Ar-NH), 6.54-7.84 (m, 12H, Ar-H), 4.14 (s, 1H, NH), 2.89-3.11 (m, 2H, -CH_2), 1.04-1.14 (m, 3H, CH_3).

***N*^{7}-(2-chlorophenyl)-*N*^{2}-(5-(4-ethoxyphenyl)-4*H*-1,2,4-triazol-3-yl)benzo[*d*]thiazole-2,7-diamine (6d):** Yield: 72%, m.p.: 244-242 ºC. R_f: 0.78. FT-IR (KBr, ν_{max}, cm^{-1}): 3473 (NH-*str*.), 1612 (C=N), 1424 (Ar-C=C), 793 (C-Cl); ^{1}H NMR (DMSO-d_6, δ ppm): 8.73 (s, 1H, Ar-NH), 6.61-7.79 (m, 12H, Ar-H), 4.04 (s, 1H, NH), 2.89-3.01 (m, 2H, -CH_2), 1.21-1.38 (m, 3H, CH_3).

***N*^{7}-(3-chlorophenyl)-*N*^{2}-(5-(4-ethoxyphenyl)-4*H*-1,2,4-triazol-3-yl)benzo[*d*]thiazole-2,7-diamine (6e):** Yield: 74%, m.p.: 226-228 ºC. R_f: 0.77. FT-IR (KBr, ν_{max}, cm^{-1}): 3469 (NH-*str*.), 1579 (C=N), 1424 (Ar-C=C), 783 (C-Cl); ^{1}H NMR

(DMSO-d_6, δ ppm): 8.86 (s, 1H, Ar-NH), 6.68-7.86 (m, 12H, Ar-H), 4.02 (s, 1H, NH), 2.90-3.07 (m, 2H, -CH_2), 1.27-1.40 (m, 3H, CH_3).

***N*⁷-(4-chlorophenyl)-*N*²-(5-(4-ethoxyphenyl)-4*H*-1,2,4-triazol-3-yl)benzo[*d*]thiazole-2,7-diamine (6f):** Yield: 73%, m.p.: 221-223 ºC. R_f: 0.90. FT-IR (KBr, ν_{max}, cm^{-1}): 3471 (NH-*str.*), 1620 (C=N), 1424 (Ar-C=C), 790 (C-Cl); ^{1}H NMR (DMSO-d_6, δ ppm): 8.83 (s, 1H, Ar-NH), 6.63-7.81 (m, 12H, Ar-H), 4.09 (s, 1H, NH), 2.94-3.02 (m, 2H, -CH_2), 1.23-1.39 (m, 3H, CH_3).

***N*²-(5-(4-ethoxyphenyl)-4*H*-1,2,4-triazol-3-yl)-*N*⁷-(piperazin-1-yl)benzo[*d*]thiazole-2,7-diamine (6g):** Yield: 76%, m.p.: 225-227 ºC. R_f: 0.80. FT-IR (KBr, ν_{max}, cm^{-1}): 3471 (NH-*str.*), 1621 (C=N), 1447 (Ar-C=C); ^{1}H NMR (DMSO-d_6, δ ppm): 9.76 (s, 1H, Ar-NH), 7.10-8.96 (m, 9H, Ar-H), 3.92 (s, 1H, NH), 3.54-3.67 (m, 2H, -CH_2), 2.56-2.77 (t, 2H, piperazine), 2.14-2.17 (t, 6H, piperazine), 1.37-1.40 (t, 3H, CH_3).

***N*²-(5-(4-ethoxyphenyl)-4*H*-1,2,4-triazol-3-yl)-*N*⁷-(4-methylpiperazin-1-yl)benzo[*d*]thiazole-2,7-diamine (6h):** Yield: 75%, m.p.: 216-218 ºC. R_f: 0.82. FT-IR (KBr, ν_{max}, cm^{-1}): 3471 (NH-*str.*), 1621 (C=N), 1447 (Ar-C=C); ^{1}H NMR (DMSO-d_6, δ ppm): 9.96 (s, 1H, Ar-NH), 7.06-7.94 (m, 8H, Ar-H), 4.02 (s, 1H, NH), 3.64-3.77 (m, 2H, -CH_2), 2.56-2.77 (t, 2H, piperazine), 2.14-2.47 (t, 6H, piperazine), 1.96 (s, 3H, -CH_3), 1.20-1.39 (t, 3H, CH_3).

***N*²-(5-(4-ethoxyphenyl)-4*H*-1,2,4-triazol-3-yl)-*N*⁷-morpholinobenzo[*d*]thiazole-2,7-diamine (6i):** Yield: 70%, m.p.: 211-214 ºC. R_f: 0.69. FT-IR (KBr, ν_{max}, cm^{-1}): 3454 (NH-*str.*), 1602 (C=N), 1421 (Ar-C=C); ^{1}H NMR (DMSO-d_6, δ ppm): 9.96 (s, 1H, Ar-NH), 7.03-7.94 (m, 8H, Ar-H), 4.04 (s, 1H, NH), 3.64-3.77 (m, 2H, -CH_2), 2.56-2.77 (m, 2H, -CH_2), 2.14-2.47 (t, 6H, morpholine), 1.96 (s, 3H, -CH_3).

***N*²-(5-(4-ethoxyphenyl)-4*H*-1,2,4-triazol-3-yl)-*N*⁷-(piperidin-1-yl)benzo[*d*]thiazole-2,7-diamine (6j):** Yield: 80%, m.p.: 213-215 ºC. R_f: 0.79. FT-IR (KBr, ν_{max}, cm^{-1}): 3454 (NH-*str.*), 3272 (Ar-CH), 1602 (C=N), 1416 (Ar-C=C). ^{1}H NMR (DMSO-d_6, δ ppm): 9.91 (s, 1H, Ar-NH), 7.02-7.92 (m, 8H, Ar-H), 4.07 (s, 1H, NH), 3.61-3.78 (m, 2H, -CH_2), 2.56-2.77 (t, 2H, piperidine), 2.09-2.39 (t, 6H, piperidine), 1.91 (s, 3H, -CH_3), 1.21-1.34 (m, 2H, CH_2).

***N*²-(5-(4-ethoxyphenyl)-4*H*-1,2,4-triazol-3-yl)-*N*⁷-(2-methylpiperidin-1-yl)benzo[*d*]thiazole-2,7-diamine (6k):** Yield: 82%, m.p.: 217-219 ºC. R_f: 0.85. FT-IR (KBr, ν_{max}, cm^{-1}): 3454 (NH-*str.*), 3079 (Ar-CH), 1601 (C=N), 1419 (Ar-C=C); ^{1}H NMR (DMSO-d_6, δ ppm): 9.96 (s, 1H, Ar-NH), 7.06-7.94 (m, 8H, Ar-H), 4.02 (s, 1H, NH), 3.64-3.77 (m, 2H, -CH_2), 2.82 (m, 1H, -CH_3), 2.56-2.77 (t, 2H, piperidine), 2.14-2.47 (t, 6H, piperidine), 1.96 (s, 3H, -CH_3), 1.20-1.39 (t, 3H, CH_3).

***N*²-(5-(4-ethoxyphenyl)-4*H*-1,2,4-triazol-3-yl)-*N*⁷-(3-methylpiperidin-1-yl)benzo[*d*]thiazole-2,7-diamine (6l):** Yield: 81%, m.p.: 218-220 ºC. R_f: 0.80. FT-IR (KBr, ν_{max}, cm^{-1}): 3454 (NH-*str.*), 3273 (Ar-CH), 1602 (C=N), 1420 (Ar-C=C); ^{1}H NMR (DMSO-d_6, δ ppm): 9.93 (s, 1H, Ar-NH), 7.12-7.87 (m, 8H, Ar-H), 4.04 (s, 1H, NH), 3.68-3.69 (m, 2H, -CH_2), 2.84 (m, 1H, -CH_3), 2.54-2.72 (t, 2H, piperidine), 2.17-2.42 (t, 6H, piperidine), 1.93 (s, 3H, -CH_3), 1.19-1.32 (t, 3H, CH_3).

Antibacterial activity: Antibacterial activity was evaluated for all the synthesised benzothiazolyl triazole derivatives (**6a-l**) on both Gram-positive (*Staphylococcus aureus* and *Bacillus subtilis*) and Gram-negative (*Escherichia coli* and *Pseudomonas aeruginosa*) bacterial strains. The inhibition of microbial growth under standardised conditions was assessed using two standardised microbial assay protocols demonstrating therapeutic efficacy of test compounds. Comparative inhibition of growth of microorganisms was measured by concentration of the compound to be tested with that produced by known concentration of a standard drug of the antibiotic having a known activity. Microbial assays were performed by cup-plate method (method A) and serial dilution method (method B). The experimental data was analysed statistically using a one-way ANOVA and Dunnett's multiple comparison test, with the ciprofloxacin group serving as the control. The results were expressed as mean ± SD and statistical significance was set at $p < 0.0332$. Data analysis was performed using GraphPad Prism® software (version 8.0.1). The GraphPad significance levels were interpreted as follows: $p \leq 0.0332$(*), $p \leq 0.0021$(**), $p \leq 0.0002$(***) and $p \leq 0.0001$ (****).

Cup-plate method (method A): The antimicrobial efficiency was determined for the antimicrobial compound that diffuse through a solid agar medium in a petri plate, typically facilitated by a well punctured into the agar using a sterile borer. As the antibiotic diffused radially outward from the well, it inhibited the microbial growth, resulting in a clear zone of inhibition surrounding the well that contains the antibiotic/test compound solution.

Serial dilution method (method B): Mueller-Hinton Broth was used to determine the MIC. The determination depended on the inhibition of growth of the microbial culture in a uniform solution of the test compound in a liquid medium that was favourable to its rapid growth in the absence of the test compound. The method determined the MIC required for the inhibition of bacterial growth at various concentrations (serial diluted in the concentration range of 100-12.5 μg/mL) for the compounds and Dilutions were prepared in DMSO, which served as the negative control.

***In silico* molecular docking analysis:**

Receptor and ligand preparation: The 3D crystal structures of the target proteins were retrieved from the UniProt server and their respective PDB IDs were downloaded from the RCSB Protein Data Bank (PDB) [11]. Missing residues were remodelled using the Swiss-Model web server and saved in PDB format [12]. Binding sites were identified through the PrankWeb server [13], after which the protein structures were processed in AutoDock Tools 1.7.1. Water molecules and heteroatoms were removed, missing amino acid residues were repaired, Kollman charges were assigned and only polar hydrogens were added. The grid box was generated using the AutoGrid utility to cover the entire receptor and the grid parameter file was saved [14]. The chemical structures were selected as ligands. Their structures were drawn in ChemDraw, converted into SMILES format and imported into Avogadro software for conversion from 2D to 3D (PDB format). Ligand structures were further processed in AutoDock Tools 1.7.1, where torsional flexibility was defined and the ligands were finally saved in PDBQT format [15].

Molecular docking with AutoDock Vina: AutoDock Vina was executed either through AutoDock Tools or *via* the command line interface. A configuration file was prepared containing the grid dimensions (x, y, z coordinates and number of grid points) corresponding to the active site of receptor, along with log and output file specifications. Upon completion, docked complexes were generated in PDBQT format for receptor–ligand interaction visualisation, while the log.txt file provided the binding affinity values [16].

Visualisation: Docking results were visualised using Biovia Discovery Studio Client 2021. The output PDBQT files of both receptor and ligand were imported into the software and interaction profiles were generated. The 3D conformations of docked complexes were saved in png format, while 2D interaction diagrams illustrating amino acid contacts with the ligands were also exported as PNG images [5].

Selection of receptors: The protein structures selected for the *in silico* antimicrobial activity study were *S. aureus* tyrosyl-tRNA synthetase (PDB ID: 5CPQ) and *E. coli* tyrosyl-tRNA synthetase co-crystallised with ligand VT1 (PDB ID: 5TZ1). These receptors were chosen due of their essential role in bacterial protein biosynthesis, where they catalyze the aminoacylation of tRNA with tyrosine, a critical step in peptide chain elongation. Inhibition of these enzymes disrupts protein synthesis, ultimately leading to bacterial growth inhibition or cell death.

ADMET prediction: The ADMETlab 2.0 web server (http://admetmesh.scbdd.com/) was accessed *via* a standard web browser. This platform integrates computational models for predicting the physico-chemical, pharmacokinetic and toxicity related properties of chemical entities.

RESULTS AND DISCUSSION

The study was aimed to design and synthesize novel antibacterial hybrids incorporating distinct pharmacophoric moieties. The desired compounds were prepared *via* a six-step synthetic protocol outlined in **Scheme-I**. Established synthetic methodologies were employed and the formation of intermediate and final compounds was confirmed using chromatographic (TLC) and spectroscopic techniques (IR, NMR and mass spectrometry). The final derivatives **6a-l** were synthesised and evaluated for their antimicrobial activity. The synthesis of compound **1** was achieved through a reaction sequence involving *m*-chloroaniline and KSCN in acetic acid, followed by bromine-mediated cyclisation to form the thiazole-fused benzene ring. The characterisation of this compound shows that the reaction was successfully achieved from the FT-IR spectrum that the peak of NH_2 and C=N appeared in the region 3390 and 1652 cm^{-1}, respectively. Also, the ^1H NMR spectrum depicted the three aromatic protons resonating in the region 7.15-7.59 and the amine (N**H**$_2$) proton appearing as a single at the δ value 7.48 ppm. The conversion of the amine to a carbamate ester was achieved by reacting compound **1** with ethyl chloroformate in the presence of pyridine at a low temperature. Pyridine, acting as a base, captured the HCl generated during the reaction and facilitated the nucleophilic attack of the amine, thus forming compound **2**. Appearance of additional C=O (C=O *str*. of carbamate ester) peak at 1732.41 cm^{-1} in IR and multiplet peaks at aliphatic region *i.e.*, δ 4.21 ppm (for -C**H**$_2$) and δ 1.37 ppm (for -C**H**$_3$) in NMR confirmed the ester formation. Hydrazide derivative, **3** (*N*-(7-chlorobenzo[*d*]thiazol-2-yl)hydrazinecarboxamide) was obtained from compound **2** *via* nucleophilic substitution mechanism. Additional NH_2 stretch at 3455.40 cm^{-1} and C=O peak at 1632.66 cm^{-1} (amide C=O *str*.) substantiates the formation of hydrazide derivative. Cyclisation of hydrazinecarboxamide (compound **3**) derivative facilitated by a base (K_2CO_3) resulted in the formation of triazole derivative **4**. Characteristic singlet CH proton on 1,2,4-triazole ring resonating at downfield region (δ 8.95 ppm) evidenced the process of cyclisation. The formation of compound **5**, 7-chloro-*N*-(5-(4-ethoxyphenyl)-4*H*-1,2,4-triazol-3-yl)benzo[*d*]thiazol-2-amine, through the reaction between the triazole carbanion of compound **4** and the carbonyl carbon of *p*-ethoxybenzoic acid, is evidenced by the disappearance of the triazole C-H proton at a δ 8.95 ppm and the appearance of additional protons in the aromatic region and aliphatic protons at the δ 3.52-3.57 (for CH_2) and 1.27-1.43 (for CH_3). Compound **5** was reacted with various substituted primary amines by nucleophilic substitution in polar aprotic solvent (DMF) to yield derivatives **6a-l**. Compared to starting material, the C-Cl stretch in the region of 758-779 cm^{-1} was absent in the FT-IR spectra and additional -NH peaks emerged in the NMR spectra at around the δ 7.08-7.32 ppm, confirming the formation of title compounds **6a-l**.

Antibacterial activity: The antibacterial activity data (Tables 1 and 2) showed that three compounds **6a**, **6e** and **6h** exhibited broad-spectrum activity at a concentration of 100 μg/mL against both Gram-positive (*S. aureus* and *B. subtilis*) and Gram-negative (*E. coli* and *P. aeruginosa*) bacteria. As the concentration decreased, their effectiveness varied. At 50 μg/mL, compounds **6a** and **6e** remained active against all tested strains except *P. aeruginosa*, while **6h** continued to show activity against all four bacterial strains. At 25 μg/mL, **6a** and **6e** retained activity only against Gram-positive bacteria, whereas **6h** showed selective activity against the Gram-negative strains *E. coli* and *P. aeruginosa* but not against the Gram-positive ones. No antibacterial activity was observed for any compound at 12.5 μg/mL. The negative control (DMSO) showed no inhibition, confirming the absence of intrinsic antibacterial activity. The positive control (ciprofloxacin) exhibited consistent inhibition against all tested strains, validating the assay. Compound **6h** showed the broadest and strongest antibacterial activity, particularly against Gram-negative bacteria, whereas compounds **6a** and **6e** were more active against Gram-positive strains (Fig. 1).

Molecular docking studies: Molecular docking analysis were performed to evaluate the binding affinities and interaction profiles of the designed compounds against two bacterial targets: *S. aureus* (PDB ID: 5CPQ) and *E. coli* (PDB ID: 5TZ1), in comparison with their respective co-crystallised ligands and ciprofloxacin as a reference (Tables 3 and 4). The docking scores ranged from -9.2 to -10.8 kcal/mol for *S. aureus* and -8.5 to -10.5 kcal/mol for *E. coli*, indicating strong binding potential across the designed molecules. Hydrogen bonding interactions were key contributors to ligand–protein stability. In *S. aureus*, residues such as GLY299, TYR297,

TABLE-1
ANTIMICROBIAL ACTIVITY DATA EXPRESSED AS ZONE OF INHIBITION;
ZONE DIAMETER (mm) ASSESSED BY CUP-PLATE METHOD

Compound	Gram-positive		Gram-negative	
	S. aureus ATCC 25923	*B. subtilis* ATCC 6633	*E. coli* ATCC 25922	*P. aeruginosa* ATCC 43288
6a	18 ± 1.15	19 ± 0.5	12 ± 1.15	11 ± 0.5
6b	NA	Not active	5 ± 0.5	Not active
6c	NA	Not active	5 ± 0.2	6.5 ± 0.57
6d	5.5 ± 0.5	6 ± 0.28	Not active	Not active
6e	17 ± 1.1	16 ± 0.57	10 ± 0.57	10 ± 0.5
6f	5 ± 0.63	7 ± 0.28	6.5 ± 0.57	5 ± 0.57
6g	5.5 ± 0.58	NA	Not active	Not active
6h	8.5 ± 0.28	9 ± 1.1	16 ± 1.15	18 ± 0.6
6i	Not active	Not active	Not active	Not active
6j	Not active	Not active	5 ± 0.5	Not active
6k	Not active	Not active	5.5 ± 0.86	Not active
6l	Not active	Not active	Not active	5.5 ± 0.6
DMSO (control)	Not active	Not active	Not active	Not active
Ciprofloxacin (std.)	21 ± 1.7	25 ± 1.38	23.5 ± 0.2	22.5 ± 0.57

TABLE-2
ANTIMICROBIAL ACTIVITY DATA EXPRESSED AS MINIMUM INHIBITORY
CONCENTRATION (μg/mL) ASSESSED BY CUP-PLATE METHOD

Conc. (μg/mL)	Gram-positive						Gram-negative					
	S. aureus			*B. subtilis*			*E. coli*			*P. aeruginosa*		
	6a	**6e**	**6h**	**6a**	**6e**	**6h**	**6a**	**6e**	**6h**	**6a**	**6e**	**6h**
100	+	+	+	+	+	+	+	+	+	+	+	+
50	+	+	+	+	+	+	+	+	+	–	–	+
25	+	+	–	+	+	–	–	–	+	–	–	+
12.5	–	–	–	–	–	–	–	–	–	–	–	–
Negative control (DMSO)	–	–	–	–	–	–	–	–	–	–	–	–
Positive control (ciprofloxacin)	+	+	+	+	+	+	+	+	+	+	+	+

TABLE-3
AMINO ACID INTERACTIONS OF DESIGNED COMPOUNDS WITH PDB:5CPQ FOR GRAM-POSITIVE BACTERIA (*S. aureus*)

Compound	Affinity (kcal/mol)	Hydrogen bonding interactions	Electrostatic interactions	Hydrophobic interactions
6a	-9.6	GLY-A:299, TRP-A:338, TYR-297	ASP-A:373	MET-A:294, PRO-A:125, PRO-A:295, ALA-A:137, VAL-A:127, ALA-A:141, VAL-A:298, GLY-A:138
6b	-10.2	TYR-B:136, GLY-B:299	–	TRP-B:338, VAL-B:127, PRO-B:295, MET-B:294, ALA-B:141, VAL-B:127
6c	-10.4	GLY-A:299, TYR-A:297, ASN-A:537	ASP-A:373	TRP-A:338, ALA-A:137, GLY-A:138, PRO-A:295, ALA-A:141, VAL-A:127, MET-A:294, PRO-A:125
6d	-10.2	GLY-B:138, TYR-B:297	–	ALA-B:141, VAL-B:127, PRO-B:125, PRO-B:295, TRP-B:338, TYR-B:136
6e	-10.8	GLY-B:138, TYR-B:297	–	PRO-B:125, VAL-B:127, MET-B:294, ALA-B:141, PRO-B:295, TRP-B:338, TYR-B:136, TRP-B:546
6f	-9.8	TRP-A:546	TRP-A:338, ASP-A:373, ASP-A:473	ALA-A:137
6g	-9.6	ASP-B:473, TYP-B:136	–	TRP-B:546
6h	-10.3	GLY-B:299, TYR-B:297	–	TRP-B:338, ALA-B:137, PRO-B:295, VAL-B:127, ALA-B:141, MET-B:294, PRO-B:125, ASP-B:473
6i	-9.2	HIS-A:472	ASP-A:373, ASP-A-473, GLU-A:420	VAL-A:326, LEU-A:422, TYR-A:136
6j	-9.5	ASP-B:473, TRP-B:546	–	THR-B:541, SER-B:134, TRP-B:338, ALA-B:137
6k	-10.3	GLY-B:138, TYR-B:297	–	PRO-B:125, VAL-B:127, MET-B:294, PRO-B:295, ALA-B:141, TRP-B:338, ASP-B:373
6l	-9.3	TRP-A:546	TRP-A:338, ASP-A:473	ALA-A:137, TYR-A136, PRO-A:539
Ciprofloxacin	-8.0	GLU-B:420	–	ASP-B:373, PRO-B:295, TRP-B:338
Co-crystal VT1	–	–	–	–

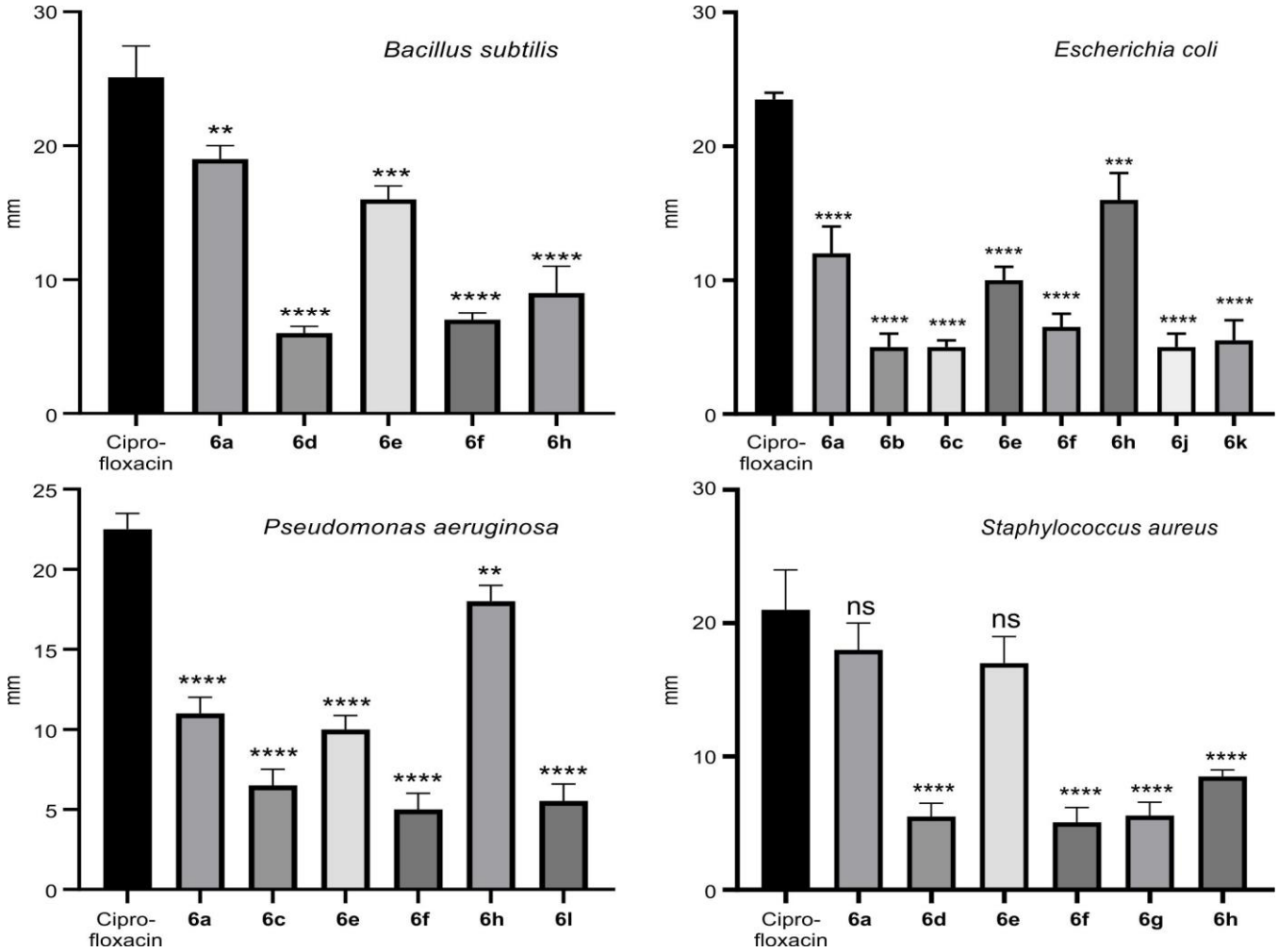

Fig. 1. Antimicrobial activities of tested compounds against Gram-positive and Gram-negative organisms with *p*-value range 0.0332(*), 0.0021(**), 0.0002(***) and 0.0001(****)

TABLE-4
AMINO ACID INTERACTIONS OF DESIGNED COMPOUNDS WITH PDB:5TZ1 FOR GRAM-NEGATIVE BACTERIA (*E. coli*)

Compound	Affinity (kcal/mol)	Hydrogen bonding interactions	Electrostatic interactions	Hydrophobic
6a	-10.3	THR-A:54, ILE-A:55	GLU-A:70	ALA-A:62, TRP-B:54
6b	-10.2	HIS-B:468	CYS-B:470	LEU-B:480, LEU-B:376, PHE-B:463, ALA-B:476, LEU-B:370, PRO-B:375, THR-B:311
6c	-9.9	SER-A:63, LYS-B:78	–	ILE-B:52, TRP-B:54, ALA-B:62, SER-B:72
6d	-10.5	TYR-A:132	PRO-A:230, MET-A:508	PHE-A:233, HIS-A:377, LEU-A:121, TYR-A:118, ILU-A:379, PRO-A:375, CYS-A:470, LEU-A:376
6e	-9.0	–	–	PHE-A:58
6f	-10.2	TYR-A:132	–	PRO-B:230, HIS-B:377, LEU-B:121, MET-B:508, LEU-B:376, CYS-B:470, PRO-B:375, THR-B:311, PHE-B:463, LEU-B:370
6g	-9.5	PHE-A:52, GLY-A:59	CYS-A:75	ALA-A:62, ILE-A:55
6h	-9.9	SER-A:63	–	ALA-B:62, TRP-B:54, ILE-A:55
6i	-8.9	HIS-B:310, ASP-B:225	–	PRO-B:193, THR-B:229, ILE-B:231
6j	-9.3	–	–	LEU-B:88, PHE-B:58, VAL-B:234, PRO-B:230, LEU-B:376, HIS-B:377, MET-B:508
6k	-10.1	SER-A:63	–	PHE-B:52, ALA-B:62, THR-B:54
6l	-9.0	LYS-B:226, ASP-B:225		PRO-B:193, ILE-B:197, ILE-B:12
Ciprofloxacin	-8.5	ALA-A:61	SER-A:507, HIS-A:377, TYR-A:505	PHE-A:233, LEU-A:87, GLY-A:65, TYR-A:64, PRO-A:230, SER-A:378
Co-crystal VT1	-11.2	ALA-A:61	PRO-A:230, TYR-A:505	TYR-A:118, LEU-A:121, PHE-A:233, SER-A:507, MET-A:508, HIS-A:377, LEU-A:88, LEU-A:87, GLY-A:65

ASN537 and ASP373 frequently engaged in hydrogen bonding, anchoring the ligands within the active site. For *E. coli*, hydrogen bonds were mainly observed with THR54, SER63, TYR132 and HIS468, further supporting high-affinity binding. Electrostatic interactions were also observed with ASP373 and ASP473 in *S. aureus* and with GLU70 and CYS470 in *E. coli*, providing additional stability through charge interactions.

Hydrophobic interactions played a prominent role in binding stabilisation for both targets. In *S. aureus*, residues such as TRP338, MET294, PRO125, ALA141 and VAL127 formed extensive hydrophobic contacts, ensuring optimal ligand positioning. Similarly, in *E. coli*, residues including PHE463, LEU376, PRO375 and MET508 created stable hydrophobic clusters around the ligands, reinforcing tight binding within the active-site pocket. These hydrophobic networks often mirrored or surpassed those of the co-crystallised ligands.

Comparative analysis with ciprofloxacin demonstrated that most of the designed compounds exhibited superior or comparable binding affinities. Notably, compound **6e** showed the strongest binding energy (-10.8 kcal/mol) against *S. aureus*. For *E. coli*, binding energies of compound **6d** showed the strongest binding energy (-10.5 kcal/mol) which was evidently close to that of the co-crystallised VT1 ligand (-11.2 kcal/ mol), suggesting potential for competitive inhibition (Fig. 2).

Evidence for selection of receptors: Structural features further support their selection, as summarised in Table-5. The crystal structures of 5CPQ and 5TZ1 possess high resolutions of 2.13 Å and 2.00 Å, respectively, enabling precise atomic-level interpretation of binding interactions. Their relatively low R-values (0.188 for 5CPQ and 0.218 for 5TZ1) indicate strong agreement between observed and calculated data, underscoring structural reliability. Moreover, these targets have been widely validated in prior antimicrobial studies, establishing their suitability as receptor models for computational screening of potential inhibitors. Their well characterised

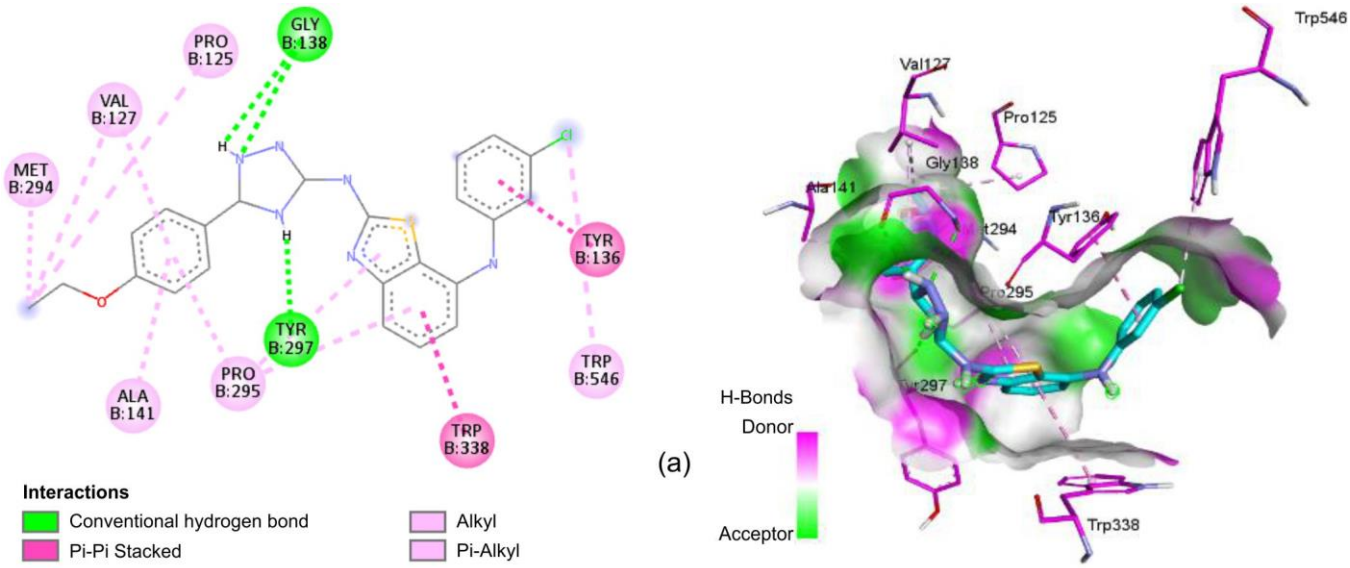

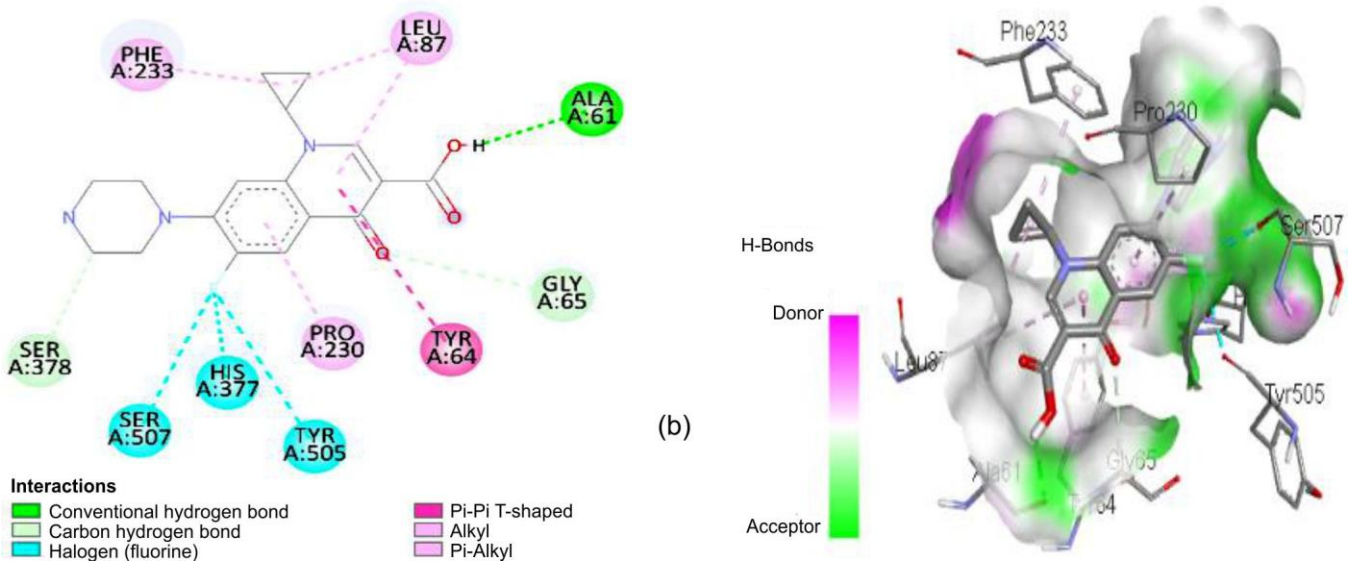

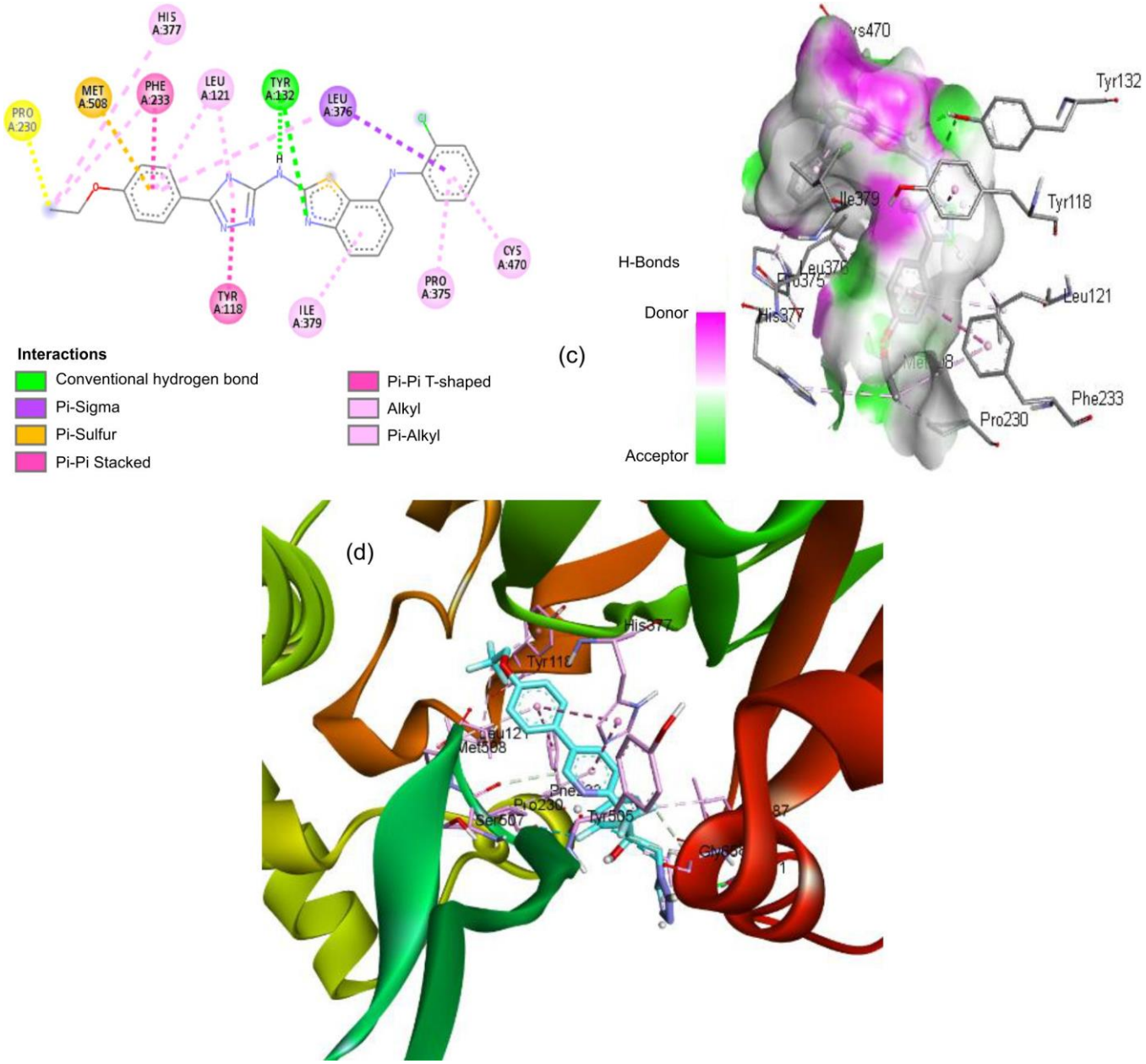

Fig. 2. 2D and 3D interaction profiles of (a) compound **6e** with 5CPQ (Gram-positive target), (b) compound **6d** with 5TZ1 (Gram-negative target), (c) ciprofloxacin with 5TZ1 and (d) 3D binding mode of co-crystallized ligand VT1 with 5TZ1

TABLE-5
SELECTED RECEPTOR TARGETS
WITH THEIR STRUCTURAL INFORMATION

Receptor	Resolution (Å)	Observed R-value	Method of collection of receptors
5TZ1	2.00	0.218	X-ray diffraction
5CPQ	2.13	0.188	X-ray diffraction

binding sites provide a robust framework for efficient docking simulations and assessment of novel ligand interactions [17-19].

ADMET studies: The ADMET evaluation of the designed compounds demonstrated that all molecules fulfilled Lipinski's rule of five, supporting their potential as orally active drug candidates. Compounds **6a-c**, with a molecular weight of 473.13 g/mol and topological polar surface area (TPSA) of 130.89 Å^2, showed high predicted gastrointestinal (GI) absorption, moderate-to-high lipophilicity (Log P: 5.915-6.001) and absence of blood–brain barrier (BBB) penetration, which may reduce central nervous system side effects.

Compounds **6d-f** (m.w.: 462.10 g/mol, TPSA: 87.75 Å^2) also exhibited high GI absorption and comparable Log P values (6.481-6.536), indicating good membrane permeability, although their lipophilicity suggests the need for careful optimisation to balance solubility. Compounds **6g-i** (m.w.: 436.18-437.16 g/mol, TPSA: 94.23-103.02 Å^2) displayed moderate lipophilicity (Log P: 3.595-4.179) with strong compliance to hydrogen bonding parameters (HBA: 9, HBD: 3-4). Compound **6j** (m.w.: 435.18 g/mol, TPSA: 90.99 Å^2) was notable for its higher hydrogen bond donor count (HBD: 8), which may influence permeability. Compounds **6k** and **6l** (m.w.: 449.20

g/mol, TPSA: 90.99 Å^2) showed similar physico-chemical profiles with Log P values of 5.175-5.486 and high GI absorption. All compounds were predicted to have low oral acute toxicity and no BBB permeability. In comparison, the reference ciprofloxacin exhibited lower molecular weight (331.13 g/mol), lower lipophilicity (Log P: -0.812) and a smaller TPSA (74.57 Å^2), highlighting the structural and physicochemical differences between the designed molecules and the standard drug.

Table-6 presents a short comparison with ciprofloxacin to interpret the ADMET results. The triazole-benzothiazole derivatives have been reported mainly for antifungal, anticancer and neuroprotective activities, with fewer reports on antibacterial effects. The current hybrids contain an ethoxyphenyl-triazole moiety and diverse N7-substituted amines to improve antibacterial potency. Notably, compounds **6a**, **6e** and **6h** demonstrated broad-spectrum activity, with **6h** exhibiting pronounced efficacy against Gram-negative strains, a feature rarely observed in prior analogues. Furthermore, *in silico* docking against tyrosyl-tRNA synthetase provides mechanistic evidence of antibacterial potential, distinguishing these hybrids from earlier triazole–benzothiazole derivatives that lacked such targeted validation. These oobservations suggest that the designed compounds possess favourable oral bioavailability profiles, with variations in lipophilicity and hydrogen bonding that may guide further optimisation for enhanced antimicrobial potential.

Structure-activity relationship (SAR): A preliminary SAR analysis suggests that the enhanced antibacterial activity of compounds **6a**, **6e** and **6h** is attributable to their distinct substituents. The nitro group in **6a** and the chloro group in **6e**, both electron-withdrawing, likely increase polarity and facilitate hydrogen bonding with bacterial enzyme residues, explaining their potency against Gram-positive strains. In contrast, the piperazine moiety in **6h** introduces a bulky, basic side chain that improves aqueous solubility and may enhance penetration through Gram-negative bacterial membranes, consistent with its broad-spectrum activity. These observations align with docking results, where these compounds exhibited stronger binding affinities compared to other analogues, supporting the role of substituent driven interactions in antibacterial efficacy.

Conclusion

This research focused on the design, synthesis and antibacterial evaluation of a novel series of 1,2,4-triazolo-benzothiazole derivatives (**6a-l**), motivated by the known pharmacological potential of both 1,2,4-triazole and benzothiazole scaffolds. The compounds were synthesised through a multistep process starting from *m*-chloroaniline and structurally characterised using TLC, IR, NMR and mass spectrometry, with key transformations such as carbamate formation, hydrazide synthesis, triazole ring construction and coupling with substituted aromatic amines confirmed by characteristic spectral features. Antibacterial screening against Gram-positive (*S. aureus*, *B. subtilis*) and Gram-negative (*E. coli*, *P. aeruginosa*) strains revealed significant activity for compounds **6a**, **6e** and **6h**, with **6h** displaying the broadest and most potent antibacterial spectrum, particularly against Gram-negative bacteria. Ciprofloxacin and DMSO were used as positive and negative controls, respectively and activity decreased with dilution, with no effect observed at 12.5 μg/mL. The molecular docking analysis demonstrated that all compounds had stronger binding affinities toward Gram-positive, *S. aureus* (-9.2 to -10.8 kcal/mol) and Gram-negative, *E. coli* (-8.9 to -10.5 kcal/mol) compared to ciprofloxacin, with compound **6e** being the most active against *S. aureus* and **6d** the most potent against *E. coli*. These enhanced scores were attributed to hydrophobic interactions with residues such as TRP338, MET294 and PRO295, along with hydrogen bonding to conserved residues including GLY299, TYR297 and ASP373. The ability of these derivatives to engage in multiple interaction types suggests greater stability and selectivity, reducing the likelihood of resistance development. The designed compounds further showed promising pharmacokinetic properties, meeting Lipinski's rule of five for orally active drugs. They also exhibited high gastrointestinal absorption, moderate to high lipophilicity and no

TABLE-6
ADMET PREDICTIONS OF SYNTHESISED COMPOUNDS (**6a-l**) COMPARED WITH STANDARD CIPROFLOXACIN

Compound	m.w.	TPSA	Log P	HBA	HBD	GI abs	BBB	Oral acute toxicity	Lip
Lipinski	≤ 500	–	≤ 5	≤ 10	≤ 5	–	–	–	–
6a	473.13	130.89	6.001	10	3	High	No	0	+
6b	473.13	130.89	5.915	10	3	High	No	0	+
6c	473.13	130.89	5.938	10	3	High	No	0	+
6d	462.1	87.75	6.481	7	3	High	No	0	+
6e	462.1	87.75	6.526	7	3	High	No	0	+
6f	462.1	87.75	6.536	7	3	High	No	0	+
6g	436.18	103.02	3.595	9	4	High	No	0	+
6h	450.2	94.23	4.018	9	3	High	No	0	+
6i	437.16	96.34	4.179	9	3	High	No	0	+
6j	435.18	90.99	5.165	8	8	High	No	0	+
6k	449.2	90.99	5.175	8	3	High	No	0	+
6l	449.2	90.99	5.486	8	3	High	No	0	+
Ciprofloxacin	331.13	74.57	-0.812	6	2	High	No	0	+

m.w.: molecular weight, TPSA: topological polar surface area (Å), Log P: partition coefficient, HBA: hydrogen bond acceptor, HBD: hydrogen bond donor, GI abs: gastrointestinal absorption, BBB: blood brain barrier, Oral acute toxicity (Category 0: low-toxicity; Category 1: high-toxicity); Lip: Lipinski rule of five (+: no violation).

blood-brain barrier penetration, which could reduce central nervous system side effects. The screened compounds also showed favourable oral bioavailability. Compounds **6a**, **6d**, **6e** and **6h** emerged as promising candidates for further *in vitro* and *in vivo* studies to evaluate their antimicrobial efficacy and safety.

ACKNOWLEDGEMENTS

The authors sincerely thank The Principal KLE College of Pharmacy for providing the necessary facilities to conduct this research work.

CONFLICT OF INTEREST

The authors declare that there is no conflict of interests regarding the publication of this article.

DECLARATION OF AI-ASSISTED TECHNOLOGIES

During the preparation of this manuscript, the authors used an AI-assisted tool(s) to improve the language. The authors reviewed and edited the content and take full responsibility for the published work.

REFERENCES

1. A.R. Shama and M.L. Savaliya, *J. Mol. Struct.*, **1337**, 142214 (2025); https://doi.org/10.1016/j.molstruc.2025.142214.
2. N. Nehra, R.K. Tittal, D.G. Vikas, Naveen and K. Lal, *J. Mol. Struct.*, **1245**, 131013 (2021); https://doi.org/10.1016/j.molstruc.2021.131013
3. S.K. Yazdana, K.L. Deepthi, B. N. Laxmi Devi, S. Afreen, S. Sibbala, B. Bhadru, M. Gudipati, V.K. Kanakaraju and N. Podila, *Egypt. J. Chem.*, **67**, 97 (2024); https://doi.org/10.21608/ejchem.2024.277247.9460
4. S. Khan, R. Hussain, Y. Khan, T. Iqbal, S. Chinnam, M. Akif and A.A. Dera, *J. Mol. Struct.*, **1318**, 139200 (2024); https://doi.org/10.1016/j.molstruc.2024.139200
5. A.M. Fahim, H.E.M. Tolan and W.A. El-Sayed, *J. Mol. Struct.*, **1251**, 131941 (2022); https://doi.org/10.1016/j.molstruc.2021.131941
6. M. Kumari, S. Tahlan, B. Narasimhan, K. Ramasamy, S.M. Lim, S.A.A. Shah, V. Mani and S. Kakkar, *BMC Chem.*, **15**, 5 (2021); https://doi.org/10.1186/s13065-020-00717-y
7. I. Ameziane El Hassani, K. Rouzi, A. Ameziane El Hassani, K. Karrouchi and M. Ansar, *Organics*, **5**, 450 (2024); https://doi.org/10.3390/org5040024
8. Y. Deswal, S. Asija, D. Kumar, D.K. Jindal, G. Chandan, V. Panwar, S. Saroya and N. Kumar, *Res. Chem. Intermed.*, **48**, 703 (2022); https://doi.org/10.1007/s11164-021-04621-5
9. K. Sudeepa, N. Narsimha, B. Aparna, S. Sreekanth, A.V. Aparna, M. Ravi, J. Mohmed and C.S. Devi, *J. Chem. Sci.*, **130**, 52 (2018); https://doi.org/10.1007/s12039-018-1437-0
10. K.P. Yadav, M.A. Rahman, S. Nishad, S.K. Maurya, M. Anas and M. Mujahid, *Intelligent Pharm.*, **1**, 122 (2023); https://doi.org/10.1016/j.ipha.2023.06.001
11. D.S. Goodsell, C. Zardecki, L. Di Costanzo, J.M. Duarte, B.P. Hudson, I. Persikova, J. Segura, C. Shao, M. Voigt, J.D. Westbrook, J.Y. Young and S.K. Burley, *Protein Sci.*, **29**, 52 (2020); https://doi.org/10.1002/pro.3730
12. A. Waterhouse, M. Bertoni, S. Bienert, G. Studer, G. Tauriello, R. Gumienny, F.T. Heer, T.A.P. de Beer, C. Rempfer, L. Bordoli, R. Lepore and T. Schwede, *Nucleic Acids Res.*, **46(W1)**, W296 (2018); https://doi.org/10.1093/nar/gky427
13. L. Jendele, R. Krivak, P. Skoda, M. Novotny and D. Hoksza, *Nucleic Acids Res.*, **47(W1)**, W345 (2019); https://doi.org/10.1093/nar/gkz424
14. G.M. Morris, R. Huey, W. Lindstrom, M.F. Sanner, R.K. Belew, D.S. Goodsell and A.J. Olson, *J. Comput. Chem.*, **30**, 2785 (2009); https://doi.org/10.1002/jcc.21256
15. O. Trott and A.J. Olson, *J. Comput. Chem.*, **31**, 455 (2010); https://doi.org/10.1002/jcc.21334
16. S. Baroroh, M. Si, U. Biotek, Z.S. Muscifa, W. Destiarani, F.G. Rohmatullah and M. Yusuf, *Indones. J. Computat. Biol.*, **2**, 22 (2023); https://doi.org/10.24198/ijcb.v2i1.46322
17. H.N. Suha, M.H. Almatarneh, R.A. Poirier and K.M. Uddin, *Int. J. Mol. Sci.*, **26**, 6752 (2025); https://doi.org/10.3390/ijms26146752
18. N. Poonia, K. Lal, A. Kumar, A. Kumar, S. Sahu, A.T.K. Baidya and R. Kumar, *Mol. Divers.*, **26**, 2375 (2022); https://doi.org/10.1007/s11030-021-10336-x
19. X. Qiu, C.A. Janson, W.W. Smith, S.M. Green, P. McDevitt, K. Johanson, P. Carter, M. Hibbs, C. Lewis, A. Chalker, A. Fosberry, J. Lalonde, J. Berge, P. Brown, C.S.V. Houge-Frydrych and R.L. Jarvest, *Protein Sci.*, **10**, 2008 (2001); https://doi.org/10.1110/ps.18001